Saturated Phase Densities of CO_2 + H_2O at Temperatures from (293 to 450) K and Pressures up to 64 MPa

Emmanuel C. Efika[1], Rayane Hoballah[1], Xuesong Li[1], Eric F. May[2,*], Manuela Nania[1], Yolanda Sanchez-Vicente[1], and J. P. Martin Trusler[1]

1. Qatar Carbonates and Carbon Storage Research Centre, Department of Chemical Engineering, Imperial College London, South Kensington Campus, London SW7 2AZ, U.K.

2. Centre for Energy, School of Mechanical & Chemical Engineering, The University of Western Australia, Crawley WA 6009, Australia

17 June 2015

Abstract

An apparatus consisting of an equilibrium cell connected to two vibrating tube densimeters and two syringe pumps was used to measure the saturated phase densities of CO_2 + H_2O at temperatures from (293 to 450) K and pressures up to 64 MPa, with estimated average standard uncertainties of 1.5 kg·m^{-3} for the CO_2-rich phase and 1.0 kg·m^{-3} for the aqueous phase. The densimeters were housed in the same thermostat as the equilibrium cell and were calibrated in-situ using pure water, CO_2 and helium. Following mixing, samples of each saturated phase were displaced sequentially at constant pressure from the equilibrium cell into the vibrating tube densimeters connected to the top (CO_2-rich phase) and bottom (aqueous phase) of the cell. The aqueous phase densities are predicted to within 3 kg·m^{-3} using empirical models for the phase compositions and partial molar volumes of each component. However, a recently developed multi-parameter equation of state (EOS) for this binary mixture [Gernert and Span, J. Chem. Thermodyn. (2015, submitted)] was found to under predict the measured aqueous phase density by up to 13 kg·m^{-3}. The density of the CO_2-rich phase was always within about 8 kg·m^{-3} of the density for pure CO_2 at the same pressure and temperature; the differences were most positive near the critical density, and became negative at temperatures above about 373 K and pressures below about 10 MPa. For this phase, the multi-parameter EOS of Gernert and Span describes the measured densities to within 5 kg·m^{-3}, whereas the computationally-efficient cubic EOS model of Spycher and Pruess [Transport in Porous Media 2010, 82, 173-196], commonly used in simulations of subsurface CO_2 sequestration, deviates from the experimental data by a maximum of about 3 kg·m^{-3}.

* Corresponding author: Eric.May@uwa.edu.au

Introduction

The amount of CO_2 that can be stored in saline aquifers depends on the saturated phase densities of mixtures of CO_2 + brines at reservoir conditions. The estimation of solubility trapping capacities requires knowledge of the aqueous phase density as a function of CO_2 concentration. Convective transport driven through the aquifer by the difference in density between the nascent brine and the layer saturated with CO_2 needs to be modelled accurately if total storage capacity is to be estimated reliably [1]. Furthermore, estimates of residual (or capillary) trapping mechanisms require robust models for interfacial tension (IFT), and standard methods of measuring IFT require knowledge of the difference in the densities of both the CO_2-rich and aqueous phases [2; 3].

Thermodynamic models used to estimate the saturated phase densities of the CO_2 + brine mixtures likely to be encountered in carbon sequestration scenarios involving saline aquifers can only be as accurate as the quality of the experimental data used in their development. Haugan et al. [4] and Jones et al. [5] stated that, ideally, the relative uncertainty of the measurements should approach 0.1 %. This is a challenging specification given the extreme nature of the conditions under which the measurements are needed. Achieving this measurement goal requires that the densimetry be both sensitive and robust, and that the experimental system used be able to prepare and manipulate a mixture without inadvertent composition changes occurring. Here we report an apparatus developed for measuring densities (but not compositions) of the aqueous and CO_2-rich phases of CO_2 + brine mixtures at saturation. In this work, we demonstrate the use of this apparatus through measurements of the baseline CO_2 + H_2O system: while the aqueous phase of this mixture has been reasonably well-studied [6; 7; 8; 9; 10; 11; 12] there are inconsistencies on the order of 1 % between some of these data sets and most of the data are restricted to temperatures below 333 K and to pressures below 30 MPa. Furthermore, there are very few experimental density data available for the CO_2-rich phase [9; 10], particularly at the requisite high pressure, high temperature conditions. A comprehensive measurement of the CO_2-rich phase density is particularly useful because the data produced will be common to all CO_2 + brine systems; one just needs to account for the change in the H_2O content of the CO_2-rich phase caused by the presence of the salt in the aqueous phase.

In the following sections we discuss some existing models available for the prediction of the saturated phase densities in CO_2 + H_2O and/or CO_2 + brine systems. We then describe the experimental apparatus used to measure the saturated densities of both phases over a wider range of conditions and/or with lower uncertainty than achieved previously. Subsequently, the results of the measurements are presented and compared with the densities of pure water and pure CO_2 at the same temperature and pressure. Finally the results are compared with data existing in the literature for this binary system, as well as with predictions made using three models developed for predicting the saturated phase densities of the aqueous and/or the CO_2-rich phases of CO_2 + H_2O.

Existing Models for Predicting Saturated Phase Densities

To calculate the density of a saturated phase, it is first necessary to obtain the phase equilibria of the mixture at the specified temperature and pressure. While there are several models in the literature available for calculating the phase equilibrium for aqueous mixtures with CO_2 [13] the correlation of Duan et al. [14] for the solubility of CO_2 in brines is one of the most widely used. This correlation was developed using aqueous phase solubility data measured over the temperature range (274 to 523) K at pressures to 200 MPa, and salt concentrations up to 4.5 mol·kg^{-1}. In this model, the water content of the CO_2-rich phase is simply calculated by applying Raoult's law to the water activity calculated for

the brine. Recently, however, Hou et al. [15] measured new vapour-liquid equilibrium (VLE) data for the CO_2 + H_2O system over the temperature range (298 to 448) K at pressures to 18 MPa, and used them to test predictions of the Duan et al. [14] correlation. Those data were represented well at $T \leq 423$ K but the correlation of Duan et al. [14] was found to over-predict the CO_2 solubility at T = 448 K by about 25 %, which is at least three times larger than its claimed uncertainty.

To facilitate sufficiently accurate calculations of phase partitioning for use in simulations of geological CO_2 sequestration, Spycher et al. [16; 17; 18] developed a simplified but computationally efficient means of calculating the phase compositions of CO_2 + H_2O and CO_2 + brine mixtures (with molalities up to 6 mol·kg^{-1}) at pressures up to 60 MPa. The impact of the non-ideality of the CO_2-rich phase on the phase equilibrium was accounted for by using the Redlich-Kwong [19] equation of state (EOS). Several simplifying assumptions were implemented to avoid the need for iterative calculations and any degradation in the performance of water-CO_2 flow models for which the solubility calculations were needed. At temperatures between (285 and 372) K [16; 17] the volume and the partial fugacity coefficient of the CO_2-rich phase were approximated to be that of pure CO_2, and the water activity was assumed to be equal to the mole fraction of water in the aqueous phase. At temperatures between (382 and 573) K, these assumptions do not allow sufficient accuracy and a Margules activity coefficient model was used to describe the aqueous phase and asymmetric binary interaction parameters that were used in the mixing rule for the Redlich-Kwong EOS to describe the CO_2-rich phase [18]. At temperatures between (372 and 382) K, this extended model [18] gives a weighted value of the properties calculated using the ideal (low temperature) and non-ideal (high-temperature) sets of correlations.

The models available for estimating the density of the aqueous phase generally calculate the partial molar volume V_2 of the CO_2 solute as a function of pressure, temperature, and brine molality; it is assumed to be independent of mole fraction x of CO_2. Treating the solvent as a pseudo-pure-component, the molar volume V_m of the solution is then obtained as follows:

$$V_{\mathrm{m}} = (1-x)V_1 + xV_2 \,. \tag{1}$$

Here, V_1, the partial molar volume of the solvent, is also assumed to be independent of the CO_2 concentration, and is calculated using an auxiliary model such as the equation of state of Wagner and Pruss [20] for pure water, or the model of Al-Ghafri et al. [21] for brines. Finally, mass density ρ of the aqueous solution containing CO_2 is obtained as follows

$$\rho = \frac{(1-x)M_1 + xM_2}{(1-x)V_1 + xV_2}, \tag{2}$$

where M_1 is the molar mass of the solvent and M_2 is the molar mass of the solute (CO_2). Sedlbauer et al. [22] presented an empirical expression for predicting the partial molar volume of various solutes (including CO_2) in pure water based on Fluctuation Solution Theory. In the case of nonelectrolyte solutes, such as CO_2, the model was tested over the temperature range (303 to 725) K at pressures to 35 MPa. Subsequently Duan et al. [23] and then Li et al. [24] presented alternative empirical correlations for the partial molar volume of CO_2 in both H_2O + CO_2 and NaCl(aq) + CO_2 mixtures at temperatures between (273 and 573) K and pressures to 100 MPa. Most recently, McBride-Wright et al. [25; 26] reported measurements of the density of under-saturated aqueous CO_2 + H_2O mixtures

using a vibrating-tube apparatus at pressures up to 100 MPa, over the temperature range (274 to 449) K, together with an empirical correlation for the partial molar volume of CO_2 that was able to represent his density data to within ±0.04 %. Partial-molar volumes predicted using the correlations of Li et al. [24] and McBride-Wright et al. [25; 26] differed by up to 7 %, whereas partial molar volumes calculated using the correlation of Sedlbauer et al. [22] had a maximum relative deviation of only 2.5 % from the model of McBride-Wright et al. [25; 26].

The density of the CO_2-rich phase in aqueous mixtures is often approximated by that of pure CO_2 at the same pressure and temperature [7]. This approximation is reasonable because the solubility of water in the CO_2 phase is much lower than that of CO_2 in an aqueous phase, and was explicitly part of the approach taken by Spycher et al. at temperatures below 373 K [16; 17]. At sufficiently low densities, the ideal gas law implies that the mass density of the CO_2 rich phase will be less than that of pure CO_2 because the molar mass of the mixture will always be less than the molar mass of pure CO_2. However, while this behaviour should be observable in the ideal gas limit, it is not clear under what conditions the impact of molecular interactions will become significant.

Duan et al. [27; 28] attempted to account for those molecular interactions by modelling both pure CO_2 and the CO_2-rich phase of mixtures using a Benedict-Webb-Rubin [29] (BWR) type equations of state. However, this work was done prior to the development of the reference EOS for CO_2 by Span and Wagner [30], which is considerably more accurate than the BWR models. Spycher et al. [16; 17; 18] regressed their RK EOS to compressibility factors for pure CO_2 calculated with the EOS of Span and Wagner [30]. The binary interaction parameters within the RK EOS mixing rule used at temperatures above 372 K were fit by Spycher et al. to phase equilibrium data for the CO_2 + H_2O system [18]. In the process of calculating the fugacity coefficients using this tuned RK EOS, the Spycher et al. [16; 17; 18] model also calculates the density of the CO_2-rich phase.

However, cubic EOS are known to give poor representations of density, especially when they are intended primarily for the description of phase equilibrium. Multi-parameter equations of state, such as those of Span and Wagner [30] for CO_2 and Wagner and Pruss [20] for H_2O, are developed to describe all thermodynamic properties for a system as accurately as possible and are increasingly being applied successfully to the description of mixtures as in, for example, the GERG-2008 EOS for natural gas [31]. Recently, Gernert and Span [32] have developed a multi-parameter EOS for the Helmholtz energy optimized for the CO_2 + H_2O system as well as other humid or CO_2-rich mixtures, referred to here as the "EOS-CG". To describe CO_2 + H_2O mixtures, the EOS-CG utilises the reference EOS for water [20] and CO_2 [30] together with a re-parameterised departure function with the same functional form as that used in the GERG-2008 EOS for natural gas [31].

Apparatus and Method

A schematic and photographs of the apparatus used in this work are shown in **Figure 1**. A Hastelloy pressure vessel (C) with an internal volume of 50 mL, containing a PTFE-coated magnetic stirrer bar and sealed with a PTFE O-ring, was housed inside a fan-forced air bath that had a long-term stability and spatial uniformity of ±0.2 K and an operating range of (293 to 473) K. To permit operation at temperatures below about 308 K, a heat exchanger (HEX) was installed within the air bath through which chilled water was circulated from an external circulating chiller (CC). A permanent magnet mounted on a motor shaft below the pressure vessel was used to rotate the stirrer inside that cell at 900 r.p.m.; as discussed below, this degree of agitation was found to be sufficient for attaining

equilibrium within approximately 10 minutes. Hastelloy tubes, each of 6.35 mm o.d. and internal volume < 1 mL, connected the top and bottom ports of the pressure vessel to one port of the corresponding vibrating U-tube densimeter (VTD) (Anton Paar, DMA-1400), that was also constructed from Hastelloy. These densimeters had an internal volume of less than 2 mL and a maximum operating pressure and temperature of 140 MPa and 473 K, respectively.

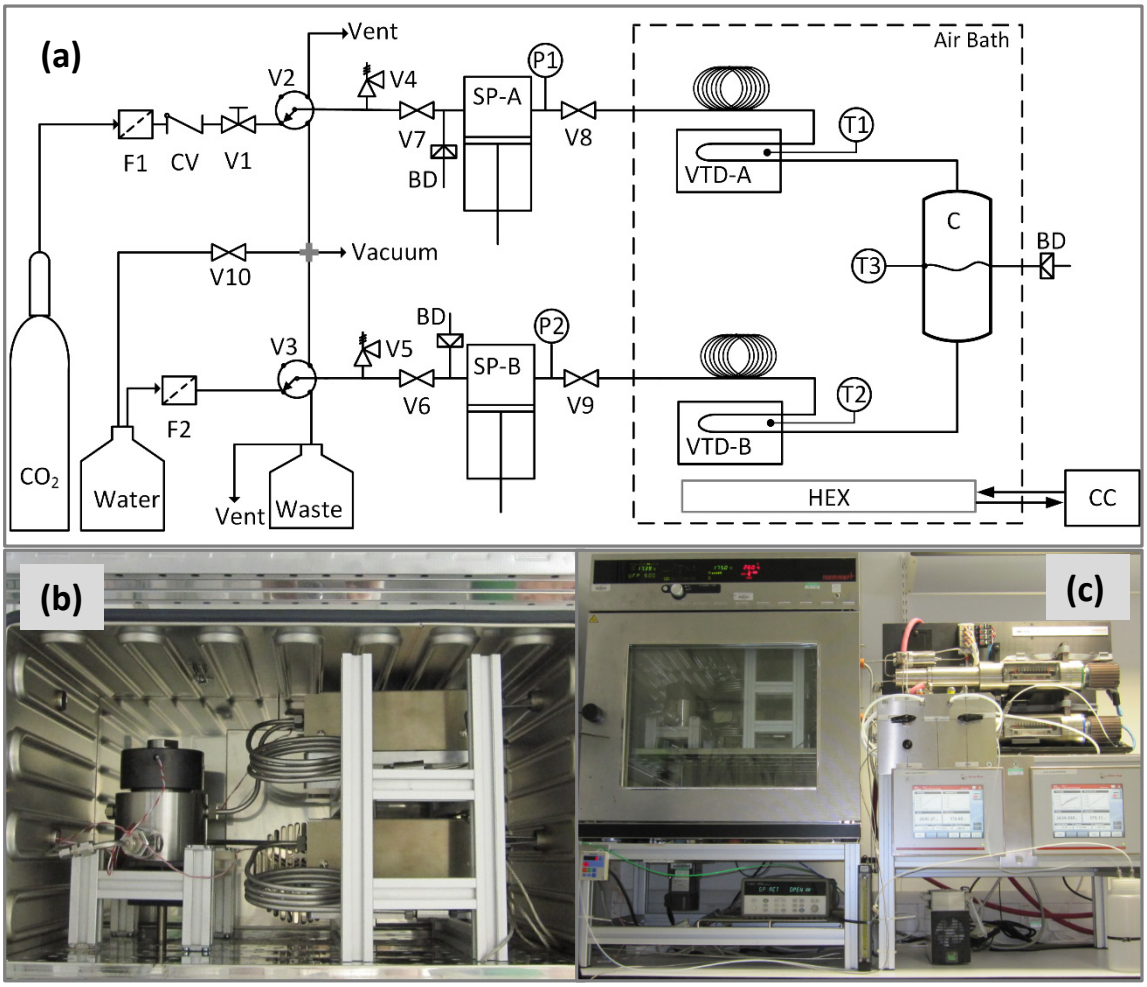

Figure 1. (a) Schematic of the apparatus: C, equilibrium vessel; VTD-A, VTD-B, vibrating-tube densimeters; SP-A, SP-B, syringe pumps; F1, F2, filters; CV, Check valve; V2, V3, 5-port valves; V4,V5, pressure relief valves; V1,V6,V7,V8,V9, isolation valves; BD; bursting disk safety devices; P1,P2, pressure transducers; T1,T2,T3, temperature sensors; HEX, heat exchanger; CC, circulating chiller. (b) Photograph showing the equilibrium cell and the two densimeters housed inside the air bath. (c) Photograph showing the air bath, syringe pumps, densimeter readouts, and ancillary equipment.

The other port of each densimeter was connected via about 6 mL of coiled Hastelloy tubing to the delivery valve (V8 or V9) of a syringe pump (SP) (Quizix model C-5000-10K) located outside the air bath. The cylinder of each syringe pump was also made of Hastelloy and had a volume at maximum extension of 10 mL. Tubing and fittings made from stainless steel or PTFE were used for all other elements of the manifold used for transferring high- or low-pressure fluids, respectively, into the pump cylinders. Syringe pump SP-A connected to VTD-A, the upper densimeter, could be filled from a cylinder containing liquid CO_2 at its saturation pressure of about 5.7 MPa via selector valve V2 and fill valve V7. A circulating chiller (not shown in Figure 1) was used to regulate the temperature of SP-A at T = 283 K to ensure any CO_2 therein remained in the liquid phase. This allowed a CO_2 sample loaded

into SP-A to be compressed up to 64 MPa when needed. The aqueous phase (de-ionised water in this work) was stored in a bottle at ambient pressure. Immediately prior to use, degassing was carried out by agitation under vacuum, the pressure in the sample bottle was restored to ambient, and the sample was drawn by suction from below the liquid surface into syringe pump SP-B via selector valve V3 and fill valve V6.

Periodically, leakage past the main PTFE O-ring seal was found to be a problem and this component then had to be replaced. This problem was attributed to swelling and subsequent decompression damage caused by dissolution of CO_2 in the polymer. All experimental data reported in this work pertain to leak-free operation of the equipment.

The system pressure was measured using the two strain-gauge type transducers (P1 and P2) (Sensata Technology, model 101HP2), one connected to each pump cylinder. By closing either of the delivery valves V8 or V9 it was possible to isolate each transducer from the other and/or from the cell. Bursting disks (BD), located in each pump and also on the equilibrium cell, were used to protect against over-pressure in the high-pressure circuit, while proportional relief valves (V4 and V5) were used to protect the filling lines to the syringe pumps. The two pressure transducers were calibrated at pressures up to 68 MPa against a reference quartz-crystal pressure gauge (Fluke, model PPCH-G-70M) with a relative uncertainty of 0.02 % of full scale (i.e. 14 kPa). The strain-gauge transducers exhibited a hysteresis of about ±30 kPa during the calibration but the mean of the pairs of readings taken with increasing and decreasing pressure were linear to with about 5 kPa. During the measurement phase, the consistency of the pressure transducer calibrations were checked by comparing the two transducers against each other when the cell contained only a single phase fluid, and by monitoring their reading when under vacuum. Periodically, the vacuum reading of the transducer in the lower cylinder (B) was observed to shift by a small amount (up to 50 kPa). However, when a new offset correction was applied to this transducer its reading remained consistent with that of the transducer in Cylinder A over the full pressure range, indicating the sensitivities of the two gauges were stable. The overall standard uncertainty of the measured pressures (including non-linearity, hysteresis, calibration uncertainty and drift) was estimated to be 50 kPa.

Three 100 Ω platinum resistance thermometers (T1, T2, T3) (PRT) were used together with a data acquisition unit/digital multimeter (Agilent, model 34970A) to measure the temperatures of the upper and lower VTD and the equilibrium cell. These were calibrated on ITS-90 over the temperature range (273 to 473) K using a triple-point-of-water cell and a standard 25 Ω PRT immersed in a stirred oil bath. The measured resistances of the 100 Ω PRTs were regressed to the ITS-90 temperatures using the Callander Van Dusen equation [33]. The resulting standard uncertainty of the thermometer calibration was 0.02 K. However, the spatial variation of temperature within the stirred air bath meant that the standard uncertainty in the temperature of the fluid phases contained within a given element was estimated to be 0.2 K.

To ensure that liquid water did not condense in the upper densimeter, a resistive heating element (not shown in **Figure 1**) was attached to the outside of the VTD housing (but inside the massive block used for vibration isolation). Approximately 5 W of DC power was used to raise the temperature of the VTD-A by around 2 K relative to the temperature of the equilibrium cell, as measured by the PRT T1 mounted in the bore of the VTD block between the U tube's inlet and outlet. This temperature shift was consistent with the independent reading from the densimeter's in-built temperature sensor,

which was monitored by the data acquisition unit supplied by the VTD manufacturer to measure the resonance period of the vibrating tube. The temperatures of the equilibrium cell and the lower VTD, as measured by the two 100 Ω PRTs, were consistent within ±0.2 K. The temperatures reported here are those of the two VTDs: phase equilibrium was achieved at the temperature of the lower VTD and this was the temperature at which the aqueous phase density was measured. However, it was necessary to measure the density of the saturated CO_2 phase at a slightly super-heated temperature.

To load a sample, the equilibrium cell, both densimeters and both syringe pumps were evacuated and flushed with CO_2 at pressures in the range (1 to 3) MPa several times, before V-9 was closed and SP-B was evacuated. Approximately 10 mL of water, freshly degassed by agitation under vacuum, was loaded into SP-B before the fill valve V6 was closed. With V6 and V9 both closed, the aqueous sample in SP-B was compressed to a pressure greater than that in the equilibrium cell before the delivery valve V9 was opened. The aqueous phase was then slowly injected through the VTD-B and into the equilibrium cell. Once the pump reached its minimum volume, the delivery valve V9 was closed and the cylinder was re-filled with a new 10 mL batch of aqueous phase. This procedure was repeated until the volume of aqueous phase in the equilibrium cell was approximately 25 mL. Further increases or decreases in system pressure were achieved by injecting or venting CO_2 through the upper syringe pump, SP-A. Following a change in pressure, it was found that approximately 10 min was required to reach equilibrium under stirring as determined by monitoring the temperature and the pressure (when the cell was isolated with V8 and V9 both closed) and/or the displacement of the piston in SP-A with SP-A in constant-pressure mode, V8 open and V9 closed.

The control software for each of the syringe pumps allowed them to be operated in either constant flow rate mode or constant pressure mode. By using one pump in constant flow mode (at a rate of 1 mL min^{-1}) and the other in constant pressure mode it was possible to manipulate the locations of the pistons in each cylinder prior to measuring the density of the saturated phases. To allow the density measurement of both phases to occur at a given pressure, it was necessary to have the pump cylinder volumes differ by at least 4 mL so that sufficient amounts of each phase could be displaced from the equilibrium cell into the corresponding VTD to completely fill it. For example, prior to a density measurement, the piston of SP-B was typically fully extended so that the volume of Cylinder B was zero, while SP-A was set to have a cylinder volume of about 8 mL. A target pressure for the entire system was chosen, and the SP-A was placed in constant pressure mode with this target as the set point; SP-B remained in constant flow mode with a set rate of zero. Once the target pressure was reached, the contents of the equilibrium cell were mixed for at least 10 minutes, the stirrer was switched off and a further five minutes was allowed before SP-B was set to withdraw at a rate of 1 mL min^{-1}. The SP-A's control algorithm maintained the system pressure by extending the piston. Usually, to maintain the pressure at the set-point, the flow rate at the upper pump was significantly larger than 1 mL min^{-1}, presumably because the compressibility of CO_2-rich phase was greater than that of the aqueous phase. After about 1.8 mL of aqueous phase sample had been withdrawn, a breakthrough curve would be observed in the resonance period time-series data being logged from the VTD-B, indicating the location and motion of the saturated aqueous phase composition front. After about 3.5 mL had been withdrawn the shift in the densimeter's resonance period was complete with any further temporal variations corresponding to any small fluctuations in overall pressure or temperature. The SP-B was stopped after between (4 and 5) mL had been withdrawn and, after a further three minutes, the resonance period of the vibrating tube was recorded over a period of one

minute. During this time SP-A, which had often injected about (6 to 8) mL to compensate for the amount withdrawn by the lower pump, remained in constant pressure mode. To be deemed stable, the standard deviation of the VTD-B's resonance period over the minute recording was required to be less than 0.01 μs.

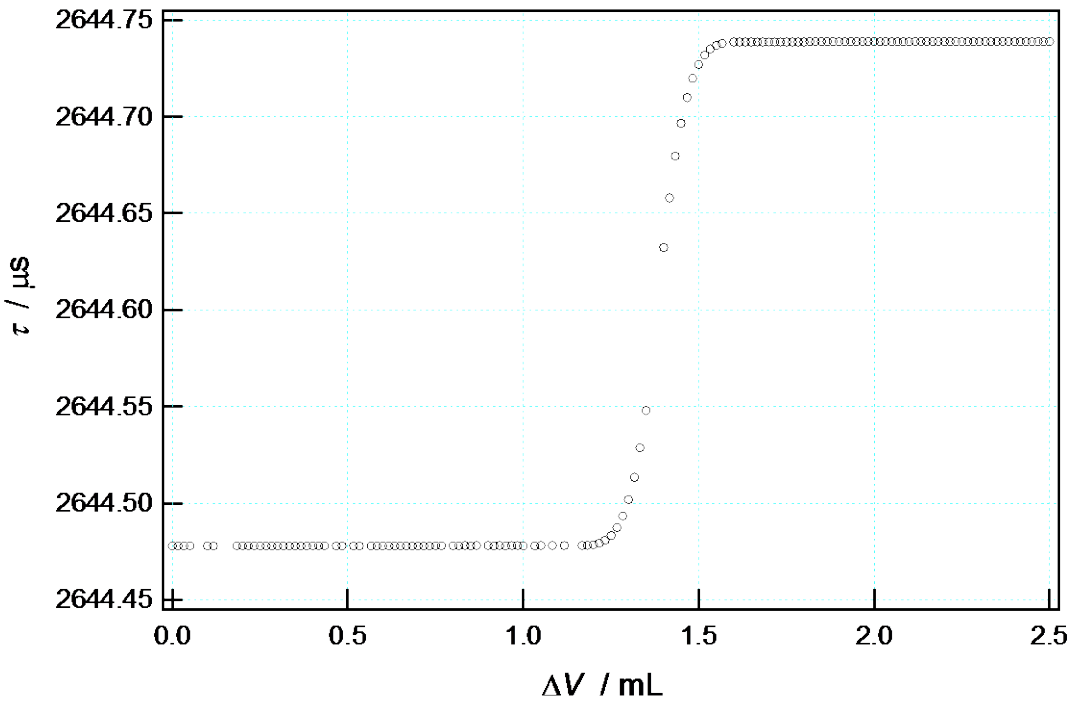

Figure 2. Breakthrough curve recorded for the upper VTD as water-saturated CO_2 was displaced into it from the equilibrium cell.

From this point, the procedure was reversed to enable the measurement of the density of the water-saturated CO_2–rich phase. The contents of the equilibrium cell were re-mixed for 10 minutes, the stirrer was switched off and a further five minutes was allowed before SP-B was set to inject at a rate of 1 mL min^{-1}. Figure 2 shows a breakthrough curve recorded as a water-saturated sample of the CO_2-rich phase was displaced from the equilibrium cell through VTD-A. At least 5 mL of the CO_2-rich phase was withdrawn in this manner, although usually the lower piston was returned to an almost fully extended position. Once the withdrawal stopped, a few minutes were allowed for equilibration before the resonance period of the VTD-A was recorded.

Prior to the mixture measurements, both densimeters were calibrated in-situ using vacuum and the pure fluids helium, CO_2 and water. The purities and other details of the sample materials used in this work are listed in Table 1. The method and results of the calibration were described by May et al:[34] the lower (VTD-B) and upper (VTD-A) densimeters used in this work correspond to VTD-2 and VTD-3 in ref. [34], respectively. The working equation used to calculate the density ρ from the measured resonance period τ was

$$\rho = \frac{\left(\rho_{\mathrm{M}}/S_{00}\right)}{\left(1+\alpha_V t+\beta_V p\right)}\left(\left(\frac{\tau}{\tau_{00}\left(1+\varepsilon_{\tau 1}t+\varepsilon_{\tau 2}t^2\right)}\right)^2\left(1+\beta_\tau p\right)-1\right) \quad , \tag{1}$$

where t is the Celsius temperature, p is the pressure, ρ_M is the density of the tube material (taken to be 8.89 g·cm^{-3}) and S_{00}, τ_{00}, $\varepsilon_{\tau 1}$, $\varepsilon_{\tau 2}$, α_V, β_V, and β_τ are apparatus parameters determined according to the calibration procedure described by May et al. [34]. Values and statistical uncertainties of the VTD parameters used in this work are listed in Table 2. Also listed are the root means square (r.m.s.) deviations of the pure fluid densities calculated using eq. (1) from the densities calculated from the reference equations of state for the pure fluids [20; 30; 35] using the measured temperature and pressure. Figure 3 shows the results of the calibration. A subsequent calibration of the densimeters using only vacuum and water and the constraint ($\beta_\tau = -\beta_V/3.87$)[34] was conducted about 8 months later and the resulting parameter values, which are also shown in Table 2, were in good agreement with the original values indicating the stability of the VTDs over that extended period.

Table 1. Material purities and suppliers.

Material	Supplier	Purity Specification
Carbon dioxide	BOC	0.9995 mole fraction
Water	MilliPore Q	Resistivity > 18 MΩ·cm at T = 298.15 K
Helium	BOC	0.99999 mole fraction

Table 2. Parameter values in eq. (1) used to convert the measured resonance periods to densities. The parameters were determined by calibration using reference EOS densities for helium, water and CO_2 as described in reference [34]. A check of that calibration was performed 8 months later using only water and helium and the constraint ($\beta_\tau = -\beta_V/3.87$) [34].

Parameter	**Lower VTD (VTD-2)**		**Upper VTD (VTD-3)**	
	Ref. [34]	This work	Ref. [34]	This work
S_{00}	$0.549715_{(75)}$	0.552041	$0.551776_{(96)}$	0.550079
τ_{00} / μs	$2578.331_{(95)}$	2577.997	$2577.964_{(62)}$	2578.203
$10^6\varepsilon_{\tau 1}$ / K^{-1}	$128.21_{(80)}$	127.50	$128.06_{(53)}$	128.55
$10^8\varepsilon_{\tau 2}$ / K^{-2}	$4.97_{(34)}$	4.99	$4.78_{(23)}$	4.87
$10^6\alpha_V$ /3 K^{-1}	$14.56_{(29)}$	14.25	$13.88_{(36)}$	14.58
$10^5\beta_V$ / MPa^{-1}	$2.56_{(41)}$	1.51	$1.87_{(52)}$	1.38
$10^5\beta_\tau$ / MPa^{-1}	$-0.321_{(18)}$	Constrained	$-0.371_{(23)}$	Constrained
$\frac{(\rho_{\mathrm{VTD}} - \rho_{\mathrm{EOS}})_{\mathrm{r.m.s.}}}{\mathrm{kg \cdot m^{-3}}}$	0.35	0.13	0.44	0.31
$10^2 \frac{(\rho_{\mathrm{VTD}} - \rho_{\mathrm{EOS}})_{\mathrm{r.m.s.}}}{\langle \rho_{\mathrm{EOS}} \rangle}$	0.071	0.013	0.089	0.032

The uncertainty of the mixture density measurements was larger than the value of 0.5 kg·m^{-3} suggested by the results of the pure fluid calibrations and the propagation of error calculation based on the uncertainties in the measured temperature, pressure and resonance period. It was instead limited by the repeatability of the mixture data: as discussed below several duplicate points were re-measured over periods ranging from six weeks to ten months. The variation between these repeat data points suggested there was an additional uncertainty contribution associated with the process of sampling and transporting the saturated phases from the equilibrium cell to the respective VTDs. Based on the consistency of the mixture density data obtained, we estimate that the uncertainty contribution due to sampling for this binary system was 1 kg·m^{-3}.

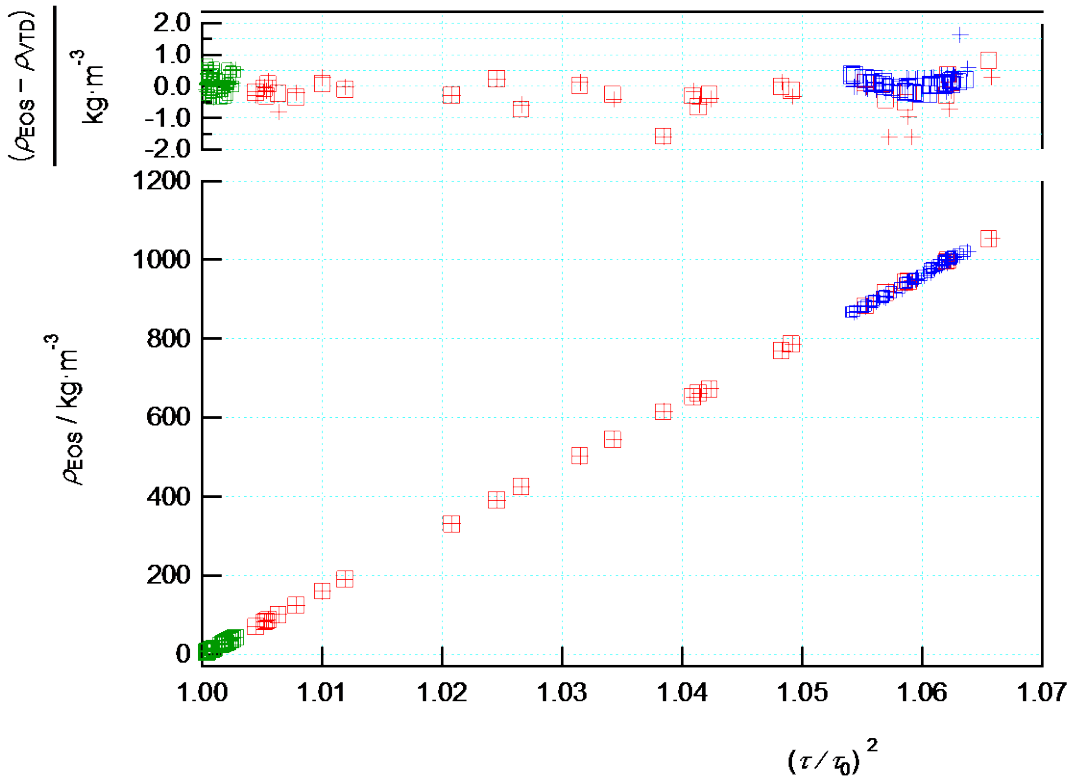

Figure 3. Lower panel: Water (blue), CO_2 (red) and helium (green) densities ρ_{EOS} calculated from their respective reference equations of state [14, 21, 24] as a function of the squared normalised resonance period $(\tau/\tau_0)^2$ measured for lower VTD(-2), □, and upper VTD(-3), +. Upper panel: Residuals between the EOS density and the density, ρ_{VTD}, calculated using eq. (1).

Results

The densities measured for the saturated aqueous and CO_2-rich phases of the CO_2 + H_2O system are listed in Table 3 and Table 4, respectively. In Table 4 both the temperature at which the phase equilibrium was established and the temperature at which the density of that phase was measured are reported. For the aqueous phase measurements (Table 3), the two temperatures were consistent within experimental uncertainty. The measured data are also presented as isothermal data series within pressure-density plots in Figure 4. The aqueous phase densities shown in Figure 4(a) vary in a near-linear fashion with pressure, although below about T = 373 K the isothermal densities exhibit a change in slope which becomes more pronounced as the temperature decreases. The (p,ρ) data for

the CO_2-rich phase shown in Figure 4(b) exhibit a more pronounced dependence on phase behaviour, similar in nature to that of pure CO_2.

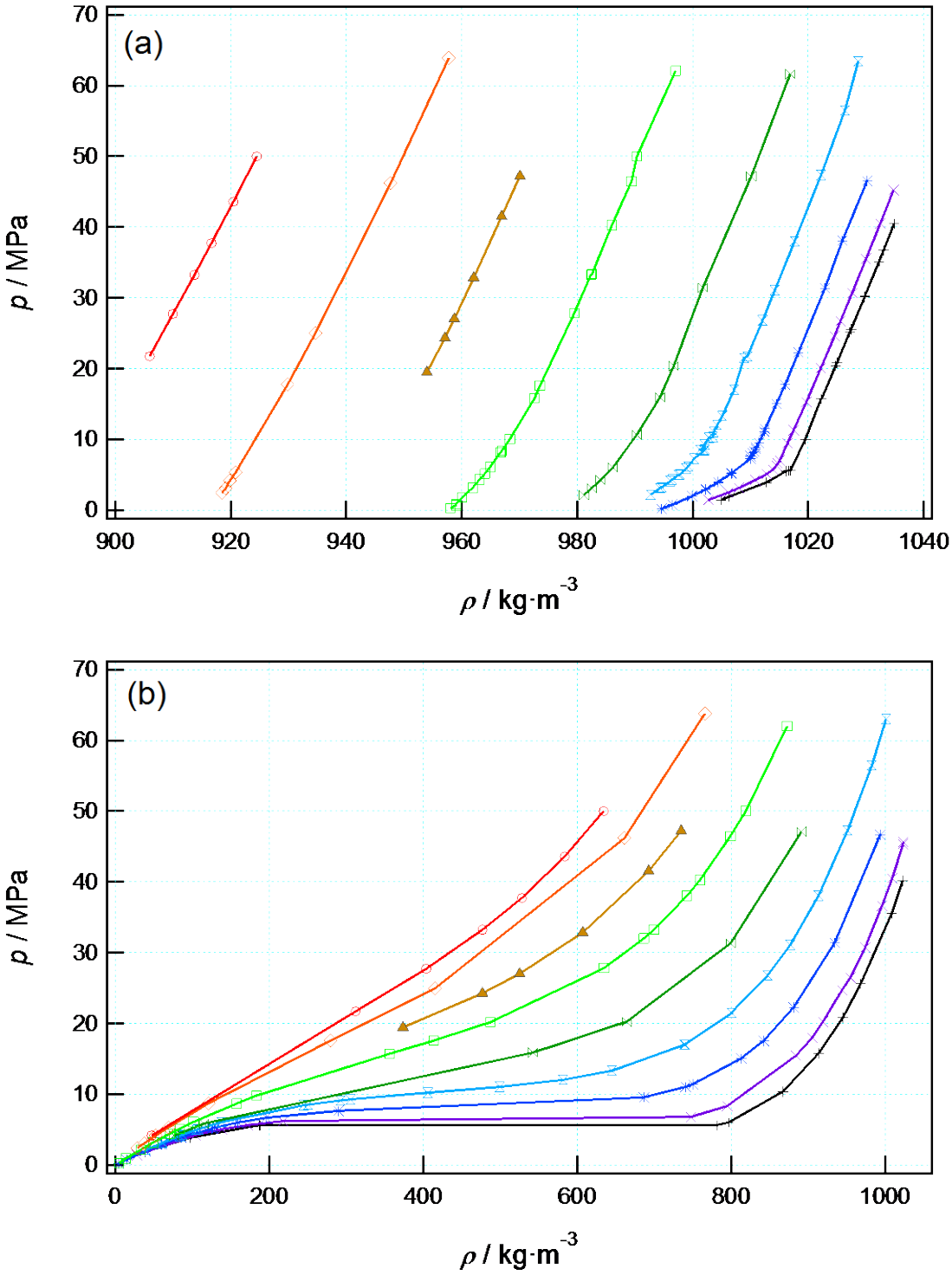

Figure 4. Measured (p, ρ) isotherm data for the CO_2 + H_2O system. (a) Aqueous phase data, for which the saturation temperature was the same as the density measurement. (b) CO_2-rich phase data, for which the saturation temperature (shown) was normally (1 to 2) K below the temperature of the density measurement (as listed in Table 4). Symbols: ┼, T = 293 K; ╳, T = 298 K; ✳, T = 308 K; ⧖, T = 323 K; ⋈, T = 343 K; □, T = 373 K; ▲, T = 398 K; ◇, T = 423 K; ○, T = 448 K. Lines are intended only to guide the eye.

Table 3. Densities ρ of the saturated aqueous phase of CO_2 + H_2O measured using the lower VTD at temperatures T_{VTD} and pressures p. The temperature of the density measurement was equal to the saturation temperature within the experimental uncertainty. Also listed is the combined standard uncertainty of each density measurement $u_c(\rho)$, which combines in quadrature the propagated uncertainties associated with T, p, sampling, and the measured resonance period. [a]

T_{VTD} / K	p / MPa	ρ / kg m^{-3}	$u_c(\rho)$ / kg m^{-3}	T_{VTD} / K	p / MPa	ρ / kg m^{-3}	$u_c(\rho)$ / kg m^{-3}
292.7	1.45	1004.9	1.0	322.8	5.91	998.8	1.0
292.7	1.87	1006.2	1.0	322.7	6.16	999.2	1.0
292.7	3.92	1012.8	1.0	322.8	7.28	1000.2	1.0
292.7	5.55	1016.2	1.0	322.7	8.44	1001.9	1.0
292.7	5.63	1016.6	1.0	322.8	8.55	1001.3	1.0
292.7	5.66	1016.9	1.0	322.7	8.57	1002.0	1.0
292.7	9.99	1019.4	1.0	322.8	9.28	1002.1	1.0
292.7	15.72	1022.2	1.0	322.8	10.25	1002.8	1.0
292.7	15.75	1022.3	1.0	322.7	10.33	1003.5	1.0
292.7	20.43	1024.7	1.0	322.8	11.05	1003.6	1.0
292.7	20.84	1025.0	1.0	322.8	12.05	1004.2	1.0
292.7	25.12	1027.2	1.0	322.8	13.34	1005.1	1.0
292.7	25.14	1027.2	1.0	322.8	17.05	1007.2	1.0
292.7	25.58	1027.4	1.0	322.8	21.53	1008.9	1.0
292.7	30.11	1029.7	1.0	322.7	21.73	1009.5	1.0
292.7	30.28	1029.8	1.0	322.7	26.83	1012.1	1.0
292.7	35.16	1032.2	1.0	322.8	31.08	1014.2	1.0
292.7	36.70	1033.0	1.0	322.8	38.03	1017.6	1.0
292.7	40.50	1034.9	1.0	322.7	47.33	1022.2	1.0
297.7	1.46	1002.7	1.0	322.8	56.51	1026.3	1.0
297.8	2.53	1006.1	1.0	322.7	63.44	1028.6	1.1
297.8	3.15	1008.0	1.0	342.8	2.15	981.1	1.0
297.8	4.25	1010.8	1.0	342.8	3.12	982.5	1.0
297.8	4.25	1010.8	1.0	342.8	4.24	984.0	1.0
297.7	5.13	1012.8	1.0	342.8	6.01	986.2	1.0
297.8	5.75	1013.9	1.0	342.8	10.65	990.3	1.0
297.8	6.31	1014.5	1.0	342.8	15.99	994.3	1.0
297.8	6.33	1014.6	1.0	342.8	20.37	996.7	1.0
297.8	6.34	1014.5	1.0	342.8	31.42	1001.7	1.0
297.8	6.65	1014.7	1.0	342.8	47.19	1010.1	1.0
297.8	7.09	1015.1	1.0	342.8	61.63	1016.9	1.0
297.8	9.45	1016.4	1.0	373.2	0.30	958.0	1.0
297.8	11.31	1017.4	1.0	373.1	0.70	959.0	1.0
297.8	15.27	1019.6	1.0	373.2	0.92	959.0	1.0
297.8	20.05	1022.2	1.0	373.2	1.82	960.0	1.0
297.8	24.65	1024.5	1.0	373.0	3.18	961.9	1.0
297.8	26.71	1025.6	1.0	373.0	4.35	963.1	1.0
297.8	30.71	1027.6	1.0	372.9	5.19	964.0	1.0
297.8	35.53	1030.0	1.0	373.0	6.13	964.9	1.0
297.8	40.49	1032.5	1.0	373.0	8.13	966.7	1.0

297.8	45.26	1034.8	1.0	373.0	8.17	966.7	1.0
307.8	0.22	994.6	1.0	373.0	8.42	966.9	1.0
307.8	0.80	996.5	1.0	373.0	10.08	968.3	1.0
307.7	2.01	999.9	1.0	373.0	15.87	972.6	1.0
307.8	2.03	999.9	1.0	373.0	17.60	973.5	1.0
307.8	2.95	1002.3	1.0	373.0	27.82	979.4	1.0
307.7	2.96	1002.2	1.0	373.0	33.24	982.3	1.0
307.7	3.94	1004.4	1.1	373.0	33.37	982.5	1.0
307.8	4.02	1004.4	1.1	373.1	40.29	986.0	1.0
307.7	5.20	1006.6	1.1	373.0	46.45	989.4	1.0
307.8	5.25	1006.7	1.1	373.0	50.01	990.3	1.0
307.7	7.27	1010.0	1.1	373.0	62.08	997.0	1.0
307.8	7.69	1010.0	1.1	398.5	19.46	954.0	1.0
307.7	8.07	1010.4	1.1	398.4	24.31	957.1	1.0
307.7	8.27	1010.6	1.1	398.4	27.05	958.7	1.0
307.8	8.62	1010.9	1.1	398.4	32.85	962.1	1.0
307.7	8.84	1010.9	1.1	398.4	41.52	966.9	1.0
307.8	9.58	1011.5	1.1	398.3	47.22	970.1	1.0
307.7	11.10	1012.4	1.1	423.3	2.43	918.5	1.0
307.8	11.48	1012.5	1.1	423.2	3.12	919.1	1.0
307.8	15.06	1014.5	1.0	423.3	4.17	919.8	1.0
307.7	17.73	1016.0	1.0	423.3	5.34	920.8	1.0
307.8	22.32	1018.3	1.0	423.2	17.73	929.8	1.0
307.7	31.36	1022.8	1.0	423.2	25.01	934.6	1.0
307.7	38.08	1025.9	1.0	423.3	46.22	947.7	1.0
307.7	46.54	1030.2	1.0	423.3	63.89	957.7	1.0
322.7	2.19	992.7	1.0	448.5	21.77	905.9	1.0
322.8	3.15	994.4	1.0	448.5	27.76	910.0	1.0
322.7	3.26	994.7	1.0	448.5	33.25	913.7	1.0
322.8	4.14	996.1	1.0	448.5	37.75	916.7	1.0
322.7	4.35	996.5	1.0	448.5	43.58	920.5	1.0
322.8	5.00	997.5	1.0	448.5	50.00	924.5	1.0
322.8	5.09	997.8	1.0				

[a] Standard uncertainties in temperature and pressure are $u(T)$ = 0.2 K and $u(p)$ = 0.05 MPa.

Table 4. Densities ρ for the near-saturated CO_2-rich phase of CO_2 + H_2O measured using the upper VTD at temperature T_{VTD} and pressure p when the phase was saturated at the same pressure but at temperature T_{sat}. Also listed is the combined standard uncertainty of each density measurement $u_c(\rho)$, which combines in quadrature the propagated uncertainties associated with T, p, sampling, and the measured resonance period. [a]

T_{sat} / K	T_{VTD} / K	p / MPa	ρ / kg m^{-3}	$u_c(\rho)$ / kg m^{-3}
292.7	292.7	1.87	38.5	1.1
292.7	292.7	3.91	97.4	1.2
292.7	292.7	5.61	187.0	2.5
292.7	293.1	5.63	187.8	2.4
292.7	292.7	5.65	781.6	2.6
292.7	292.7	5.65	781.1	2.6
292.7	292.8	6.04	796.2	2.9
292.7	292.5	10.40	867.0	1.7
292.7	292.7	15.78	913.3	1.4
292.7	292.7	15.81	913.4	1.4
292.7	292.7	20.85	944.9	1.3
292.7	292.7	25.60	968.2	1.3
292.7	292.8	35.55	1008.1	1.2
292.7	292.8	40.18	1022.5	1.2
297.8	297.8	1.42	27.7	1.1
297.8	297.8	4.24	103.8	1.2
297.8	297.8	4.24	103.8	1.2
297.8	297.8	5.08	138.5	1.4
297.8	297.8	5.68	172.0	1.8
297.8	297.8	6.21	217.8	3.0
297.8	297.8	6.79	747.5	3.9
297.8	297.8	8.33	794.5	2.4
297.8	297.8	15.45	884.0	1.5
297.8	297.8	17.97	904.9	1.4
297.8	297.8	20.25	918.8	1.4
297.8	297.8	24.73	944.1	1.3
297.8	297.8	26.52	954.6	1.3
297.8	297.8	30.75	973.7	1.2
297.8	297.8	36.61	995.4	1.2
297.8	297.8	40.49	1008.7	1.2
297.8	297.8	45.34	1023.0	1.2
297.8	297.8	45.59	1023.4	1.2
307.7	308.7	0.25	4.2	1.1
307.7	308.9	0.79	14.8	1.1
307.7	308.9	0.80	14.9	1.1
307.7	309.1	2.00	39.2	1.1
307.7	308.9	2.01	38.7	1.1
307.7	308.8	2.92	59.1	1.1
307.7	309.0	2.94	60.1	1.1
322.8	323.9	9.12	291.8	2.4
322.8	323.9	9.28	305.3	2.6
322.8	323.9	10.25	406.0	4.2
322.8	323.9	11.05	499.1	4.6
322.8	323.8	12.05	581.6	3.6
322.8	323.9	13.34	645.2	2.7
322.8	323.7	17.05	740.2	1.8
322.8	323.9	17.05	739.2	1.8
322.8	323.8	21.49	800.5	1.5
322.8	324.1	21.52	799.9	1.5
322.8	324.1	26.81	847.0	1.3
322.8	323.8	31.10	876.3	1.3
322.8	323.8	38.05	913.1	1.2
322.8	324.1	47.31	951.2	1.2
322.8	323.8	56.48	982.4	1.1
322.8	324.1	63.01	1000.7	1.1
342.8	344.2	4.16	76.2	1.1
342.8	344.2	5.88	115.2	1.1
342.8	344.2	15.90	542.5	2.1
342.8	344.2	20.28	664.2	1.7
342.8	344.2	31.37	799.0	1.3
342.8	344.2	47.11	891.3	1.2
373.0	374.1	0.30	4.6	1.0
373.0	374.1	0.93	13.8	1.1
373.0	374.4	2.15	32.7	1.1
373.0	374.4	3.17	49.1	1.1
373.0	374.4	4.44	71.0	1.1
373.0	374.3	5.14	83.7	1.1
373.0	374.4	6.09	101.7	1.1
373.0	374.4	8.71	157.6	1.1
373.0	374.4	9.78	183.1	1.1
373.0	374.3	15.76	356.7	1.4
373.0	374.1	17.59	413.2	1.4
373.0	374.1	20.20	487.0	1.5
373.0	374.1	27.82	634.6	1.4
373.0	374.1	32.04	686.7	1.3
373.0	374.1	33.24	699.4	1.3
373.0	374.1	38.04	742.5	1.2
373.0	374.1	40.30	759.5	1.2

307.7	309.0	3.92	85.7	1.2
307.7	308.8	3.98	86.3	1.2
307.7	309.1	5.17	125.6	1.3
307.7	308.8	5.24	126.5	1.3
307.7	308.8	6.02	159.0	1.4
307.7	308.8	6.70	196.1	1.8
307.7	308.8	7.68	290.3	4.8
307.7	308.9	9.58	686.0	3.7
307.7	309.0	11.04	740.4	2.5
307.7	308.9	11.45	750.5	2.3
307.7	308.9	15.06	812.5	1.7
307.7	309.0	17.61	842.0	1.5
307.7	308.9	22.32	881.2	1.4
307.7	309.1	31.40	934.0	1.3
307.7	309.1	46.68	993.5	1.2
322.8	324.2	2.16	39.5	1.1
322.8	323.9	3.15	61.2	1.1
322.8	324.1	3.20	61.3	1.1
322.8	323.9	4.15	83.7	1.1
322.8	324.1	4.28	86.9	1.1
322.8	323.8	5.00	105.8	1.2
322.8	324.1	5.07	107.9	1.2
322.8	324.1	6.05	137.7	1.2
322.8	324.1	8.45	244.8	1.8
322.8	323.9	8.55	250.2	1.9
373.0	374.4	46.46	798.9	1.2
373.0	374.1	50.04	819.1	1.2
373.0	374.4	62.00	872.4	1.1
398.4	399.4	19.44	373.7	1.2
398.4	399.3	24.29	476.7	1.3
398.4	399.3	27.04	525.3	1.3
398.4	399.4	32.84	607.1	1.2
398.4	399.3	41.54	692.6	1.2
398.4	399.2	47.24	734.7	1.2
423.3	424.8	2.42	28.4	1.0
423.3	424.8	3.11	37.8	1.0
423.3	424.9	4.17	52.4	1.0
423.3	424.8	5.32	69.0	1.0
423.3	424.8	8.73	121.3	1.1
423.3	424.8	17.59	279.8	1.1
423.3	424.8	24.98	415.6	1.2
423.3	424.9	46.18	661.4	1.1
423.3	424.9	63.77	765.7	1.1
448.5	449.5	4.18	47.1	1.0
448.5	449.5	21.74	312.4	1.1
448.5	449.5	27.74	403.8	1.1
448.5	449.5	33.24	476.9	1.1
448.5	449.5	37.74	527.9	1.1
448.5	449.5	43.58	583.6	1.1
448.5	449.6	50.01	634.0	1.1

[a] Standard uncertainties in temperature and pressure are $u(T)$ = 0.2 K and $u(p)$ = 0.05 MPa.

Discussion

Since no composition measurements were made in this work, comparisons are made below with models (or combinations of models) that permit the saturated-phase densities to be calculated at specified temperatures and pressures.

Aqueous phase of CO_2 + H_2O

The absolute densities plotted in Figure 4 reflect primarily the dependence of the parent phase density on pressure as a function of temperature. The contribution of the minor component on the saturated mixture density is better assessed by considering the differences in density between the mixture and that of either pure water (for the aqueous phase) or pure CO_2 (for the CO_2-rich phase). Figure 5 shows the differences between the measured CO_2-saturated aqueous phase densities from those of pure water at the same temperature and pressure, calculated using the reference EOS for water of Wagner and Pruss [20]. On this scale, some scatter in the measured data is evident but this is consistent with the estimated densities uncertainties listed for the aqueous phase in Table 3, which have an average of 1.0 kg·m^{-3}. The change of slope at pressures near 10 MPa for isotherms below the critical temperature of CO_2 is very clear in Figure 5, and represents the transition from vapour-liquid equilibrium at low pressures, where the CO_2-solubility approximately follows Henry's law, to liquid-liquid equilibrium at high pressures.

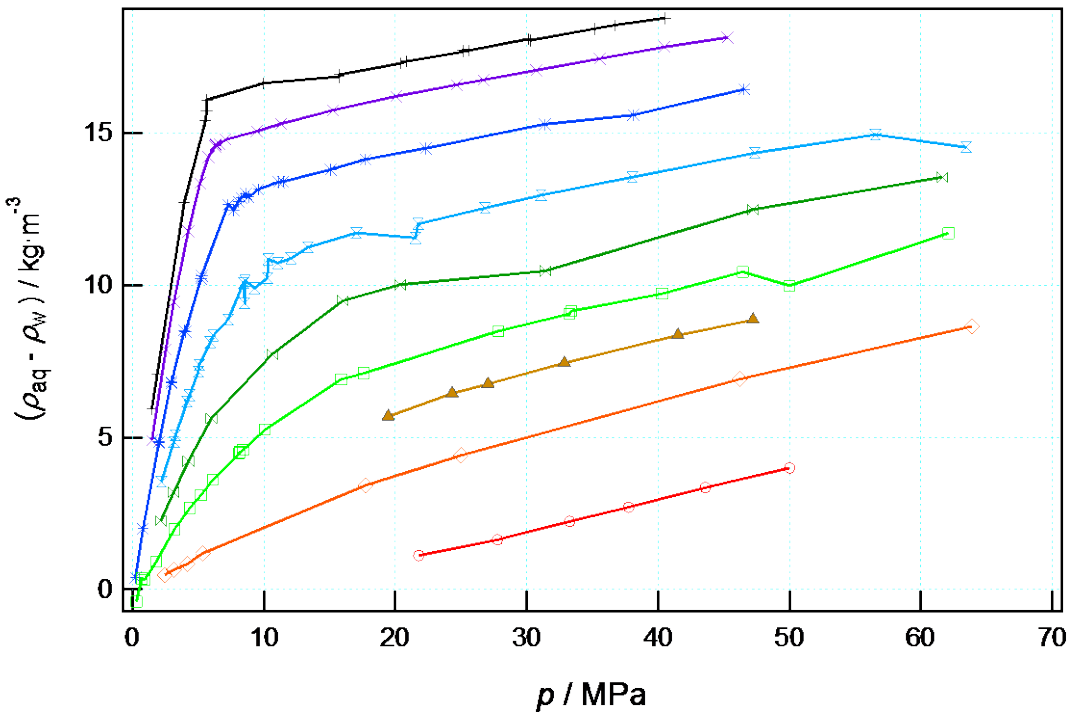

Figure 5. Differences between the measured aqueous phase densities ρ_{aq} for CO_2 + H_2O from the density ρ_w of pure water at the same pressure and temperature as calculated using the EOS of Wagner and Pruss [20]. Symbols: ┼, T = 293 K; ×, T = 298 K; ✳, T = 308 K; ⧖, T = 323 K; ⋈, T = 343 K; □, T = 373 K; ▲, T = 398 K; ◇, T = 423 K; ○, T = 448 K. Lines are intended only to guide the eye.

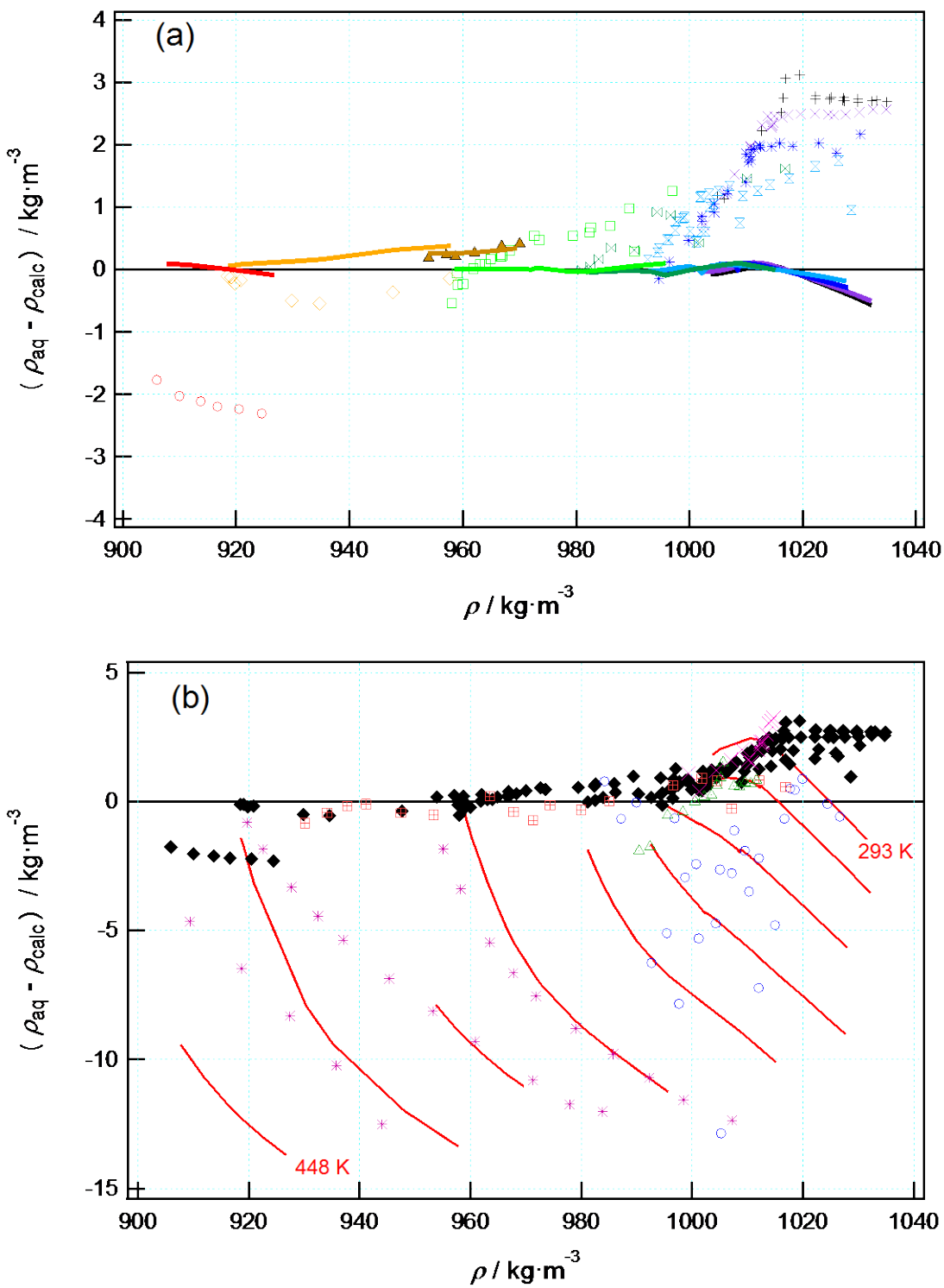

Figure 6. Deviations (ρ_{aq} - ρ_{calc}) of the saturated aqueous-phase densities ρ_{aq} for the CO_2 + H_2O system from values ρ_{calc} calculated at the same temperature and pressure using the models of Duan et al. [14] (for saturated phase composition), Sedlbauer et al. [22] (for CO_2 partial molar volume) and Wagner and Pruss [20] (for solvent molar volume). (a) Symbols: this work ┼, T = 293 K; ╳, T = 298 K; ✳, T = 308 K; ⧖, T = 323 K; ⋈, T = 343 K; □, T = 373 K; ▲, T = 398 K; ◇, T = 423 K; ○, T = 448 K. Curves: ρ_{aq} predicted using the EOS of Spycher et al. [16],[18] (for saturated phase composition) in place of the Duan et al. [14] at the experimental conditions studied in this work. (b) Symbols: ◆, this work; ○, Chiquet et al. [9]; ⊞, Yan et al. [36]; △, Hebach et al. [7]; ✳,Tabasinejad et al. [10]; ╳, Yaginuma et

al. [11]. Curves: ρ_{aq} predicted (entirely) with the EOS-CG of Span and co-workers [32] at the experimental conditions studied in this work.

Figure 6 shows the deviations of the measured CO_2-saturated aqueous-phase densities, ρ_{aq}, from those calculated, ρ_{calc}, using the empirical models of Duan et al. [14] (for saturated phase composition), Sedlbauer et al. [22] (for CO_2 partial molar volume) and Wagner and Pruss [20] (for solvent molar volume). The deviations, which are all within the experimental uncertainty, indicate that this combination of models is capable of describing the saturated aqueous-phase densities of this well - studied system as accurately as they can currently be measured. The largest deviations occur at low temperatures and high pressures, where the difference between the mixture and pure water densities is largest (but still only 20 kg·m^{-3}). At the highest temperature measured here (448 K) the deviations from the model are of a similar magnitude but the opposite sign. Figure 6(a) also shows the effect of replacing the model of Duan et al. [14] with the EOS of Spycher et al. [16; 18] for prediction of the saturated phase composition in the calculation of ρ_{calc}. The differences are almost negligible, ranging from (-0.6 to 0.4) kg·m^{-3}.

Figure 6(b) shows how data available in the literature for the aqueous phase densities of the CO_2 + H_2O binary compare with the new data, as well as densities calculated using the EOS-CG of Gernert and Span [32]. The new data extend, and are consistent with, the data sets reported by Hebach et al. [7], Yan et al. [25] and Yaginuma et al. [11], which have a similar degree of scatter to the current work. In contrast, the data of Chiquet et al. [9] have relative deviations of as much as -1.2 % from the calculated densities, with an average of -0.3 % and a standard deviation of 0.3 %, which is about three times larger than the standard deviation of the data reported here. The densities reported by Tabasinejad et al. [10] at T = (382, 423 and 468) K have low scatter and are consistent with the other data and the model predictions at their lowest pressure around 3.5 MPa. However, the data exhibit a systematic negative deviation with increasing pressure that exceeds -1 % at all three temperatures. Additionally, the data of Nighswander et al. [12], which are not plotted in Figure 6(b), deviate by between -1 % and -3 %.

The value of the new data reported here for the aqueous phase densities is highlighted by the comparison in Figure 6(b) of the recently developed EOS-CG of Gernert and Span [32] with the literature density data. The new experimental results presented here help resolve the ambiguity associated with the inconsistency in the literature data and demonstrate that the data sets of Chiquet et al. [9], Tabasinejad et al. [10] and Nighswander et al. [12] should not be weighted highly in the development of future models.

CO_2-rich phase

The density of the CO_2-rich phase is even closer to that of pure CO_2 than the aqueous phase density is to pure water. Figure 7(a) shows the deviations of the (near)-saturated CO_2-rich phase densities from those of pure CO_2 at the same temperature and pressure, calculated using the reference EOS for carbon dioxide of Span and Wagner [30].

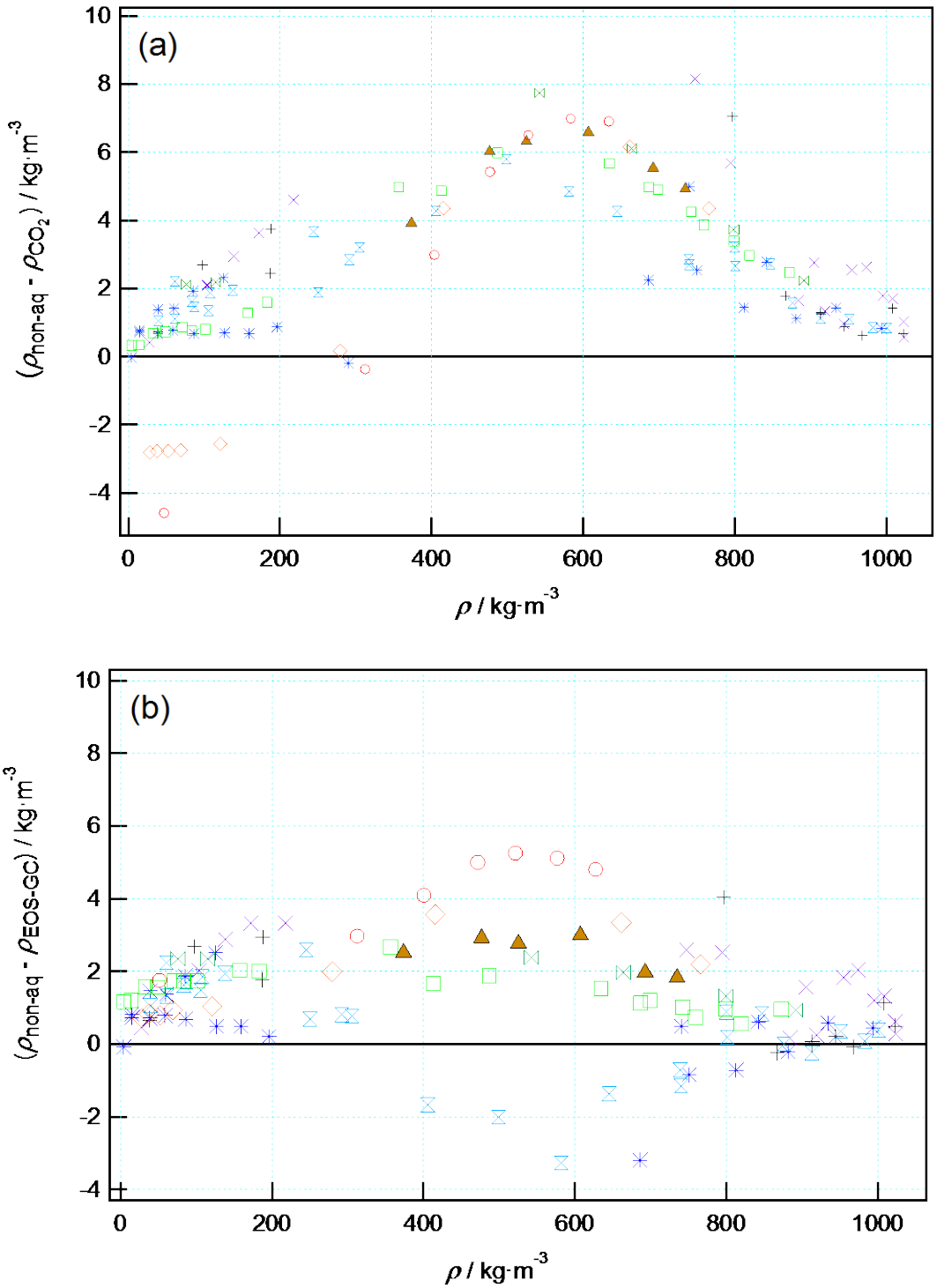

Figure 7. (a) Differences between the measured densities $\rho_{non\text{-}aq}$ of the CO_2-rich phase from the density ρ_{CO_2} of pure CO_2 at T_{VTD} as calculated from the EOS of Span and Wagner [30]. (b) Deviations ($\rho_{non\text{-}aq}$ - $\rho_{EOS\text{-}CG}$), where $\rho_{EOS\text{-}CG}$ is the density of the CO_2-rich phase calculated using the EOS-GC of Gernert and Span [32]. The $\rho_{EOS\text{-}CG}$ values used T_{sat} in Table 4 to predict the mixture composition and then used T_{VTD} ($\approx T_{sat}$ + 1 K) to calculate the density of that mixture at the measurement temperature. Symbols: ┼, T_{VTD} = 293 K; ╳, T_{VTD} = 298 K; ✳, T_{VTD} = 309 K; ⧖, T_{VTD} = 324 K; ⋈, T_{VTD} = 344 K; □, T_{VTD} = 374 K; ▲, T_{VTD} = 399 K; ◇, T_{VTD} = 425 K; ○, T_{VTD} = 450 K.

In the limits of both high and low densities, the deviations of the mixture mass densities from those of pure CO_2 tend to zero, except at the two higher temperatures, 425 K and 450 K, where the deviations become negative as expected from ideal-gas mixing (because the molar mass of H_2O is lower than that of CO_2). At lower temperatures, the vapour pressure of water and, hence, the mole fraction of water in the CO_2-rich phase is small, and thus it might be expected that any reduction of the mixture's density relative to pure CO_2 due to ideal-gas mixing would be smaller than the resolution of the experiment. However, at these lower temperatures the mixture becomes denser than pure CO_2 with the effect being clearly larger than the experimental uncertainty at densities above about 100 kg·m^{-3}. This indicates that the small decrease in the mixture's molar mass at these conditions is offset by a slightly larger increase in the mixture's molar density. Above about 800 kg·m^{-3}, where the CO_2-rich mixture has reached molar densities characteristic of a liquid phase, the decrease in the mixture's molar mass at all temperatures appears to be nearly balanced by the molar density increase. Between these two limits, the mixture densities deviate positively from those of pure CO_2, with a maximum of about 8 kg·m^{-3} across all measurements. The location and value of the maximum appears to vary with temperature: at the lower temperatures it is in the vicinity of the critical density for CO_2 (468 kg·m^{-3}) [30], whereas at the highest temperature, it has shifted to around 600 kg·m^{-3}. It is apparent from this maximum that at near-critical densities the mixture can support a molar density that more than offsets the associated decrease in molar mass.

Figure 7(b) compares the new data for the CO_2-rich phase with mixture densities, $\rho_{\text{EOS-CG}}$, calculated using the EOS-CG of Gernert and Span [32]. To calculate $\rho_{\text{EOS-CG}}$, the EOS-CG was first used to calculate the saturated phase composition at T_{sat} in Table 4 and then again to calculate the density of this mixture at T_{VTD} in Table 4 (where it is slightly under-saturated). While the difference between T_{sat} and T_{VTD} in Table 4 is small (≈ 1 K to 2 K), the sensitivity of density to temperature in the vicinity of carbon dioxide's critical point means that assuming $T_{\text{VTD}} = T_{\text{sat}}$ for data around 500 kg·m^{-3} in the range (308 to 344) K causes $\rho_{\text{EOS-CG}}$ to shift by (10 to 30) kg·m^{-3}. The maximum and r.m.s. deviations of multi-parameter EOS-GC from the data are 5 kg·m^{-3} and 2 kg·m^{-3}, respectively; the data have a standard deviation about the model predictions of 1.5 kg·m^{-3}, which is close to the average experimental combined standard uncertainty for the CO_2-rich phase. In contrast, the GERG-2008 multi-parameter EOS [31] which was developed for natural gas mixtures, has maximum and r.m.s. deviations from the data of 23 kg·m^{-3} and 6 kg·m^{-3}, respectively, while the EOS for pure CO_2 by Span and Wagner [30] has maximum and r.m.s. deviations of 8 kg·m^{-3} and 3 kg·m^{-3}, respectively.

Figure 8 shows a comparison of the results from this work with the other two sets of density data available in the literature for the CO_2-rich phase. The data of Chiquet et al. [9], which cover the temperature range (307 to 384) K again exhibit the most scatter, with a range of 49 kg·m^{-3} and a standard deviation of 8 kg·m^{-3}. Three of the four isotherms reported by Tabasinejad et al. [10] have a similar scatter to the data reported here, and also have a maximum positive difference from the density of pure CO_2 in the vicinity of its critical density, although this difference is about twice as large in magnitude as observed in this work. However, data on one of the intermediate isotherms measured by Tabasinejad et al. [10] appear to be inconsistent with their other data and those measured in this work, with an apparent minimum of similar magnitude also occurring near the critical density. At higher densities, the deviations increase linearly, reaching nearly 60 kg·m^{-3}. It is likely this subset of the measurements by Tabasinejad et al. [10] suffer from a systematic error and should be excluded from further consideration.

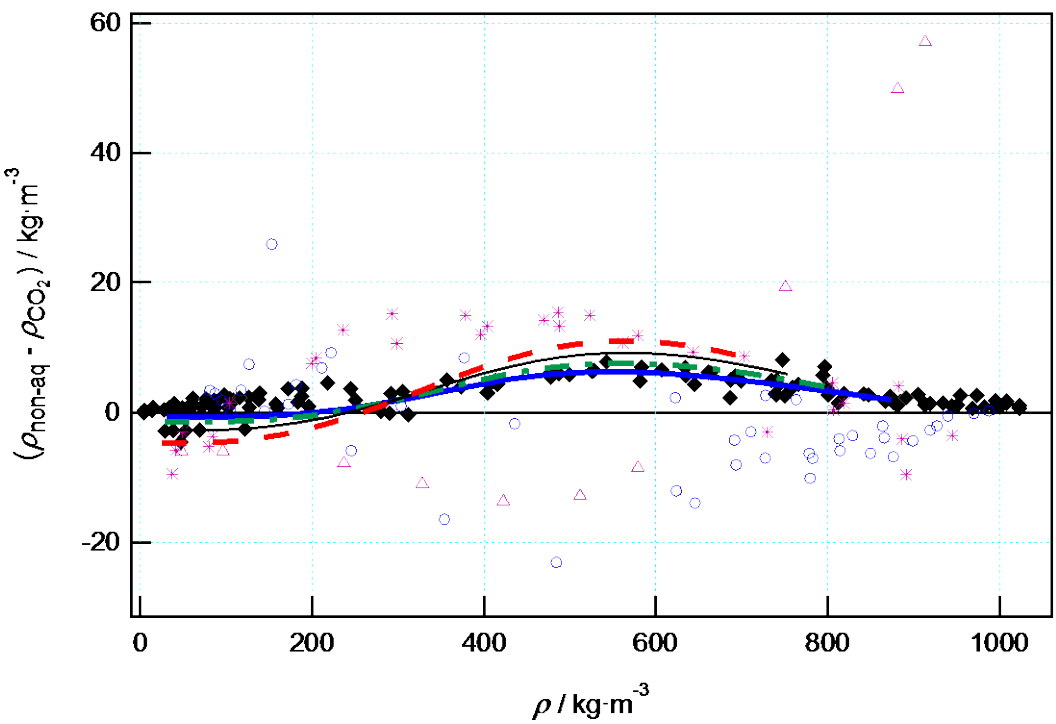

Figure 8. Differences between the densities $\rho_{non\text{-}aq}$ of the CO_2-rich phase from the density ρ_{CO_2} of pure CO_2 as calculated from the EOS of Span and Wagner [30]. Symbols: ✳, Tabasinejad et al. [10] at T = (423, 462 and 478) K; △, Tabasinejad et al. [10] at T = 446 K; ○, Chiquet et al. [9]; ◆, this work (with ρ_{CO_2} evaluated at T_{VTD}). Curves show calculations made using the EOS of Spycher and Pruess [18] at: ——, T = 373 K; — · —, T = 398 K; ——, T = 423 K; — —, T = 448 K.

Figure 8 also shows a comparison of CO_2-rich phase densities calculated using the RK-EOS within the model of Spycher and Pruess [18]. At temperatures below 372 K, this model explicitly treats the CO_2-rich phase as pure CO_2, so only comparisons for the isotherms measured in this work at higher temperatures are shown. Between (372 and 382) K, densities calculated using the model of Spycher and Pruess [18] are a weighted average of the RK-EOS predictions for pure CO_2 and the water-saturated mixture. At each of the four temperatures above 372 K considered, the CO_2-rich phase densities calculated using the model of Spycher and Pruess [18] are in remarkably good agreement with the experimental results obtained in this work. At 373 K, the cubic RK-EOS predicts a maximum density difference from pure CO_2 of +6 kg·m^{-3} at a density of around 540 kg·m^{-3}, which is consistent with the measured differences within the experimental uncertainty. The location of the predicted maximum does not change significantly with temperature, although the value of the predicted maximum difference does increase systematically with temperature up to +11 kg·m^{-3} at 448 K. Furthermore, the model correctly predicts the density differences observed in the limit of both low- and high-density limits, including the negative density differences observed at lower pressures and higher temperatures.

Conclusions

A new apparatus capable of precise measurements of the saturated densities of both the aqueous and CO_2-rich phases over a wide range of temperature and pressure has been described and demonstrated. Measurements made for both the saturated aqueous phase and CO_2-rich phase of the $CO_2 + H_2O$ system over the temperature range (293 to 450) K at pressures to 64 MPa helped identify

erroneous literature data and extend the range of the available accurate literature data. For the saturated aqueous phase of the CO_2 + water system, the new data were consistent with two existing data sets [7; 25] that exhibit comparable uncertainties and with the predictions of an empirical model [14; 20; 22] to within 0.3 % of the density. Using the computationally efficient EOS of Spycher et al. [16; 18] to calculate the aqueous phase composition in the empirical model rather than the method of Duan et al. [14] produced negligibly different results. However, the EOS-CG model developed recently by Gernert and Span [32] reproduces one of the erroneous data sets [10] and its predictions for the aqueous phase density of the $CO_2 + H_2O$ system deviated systematically with increasing pressure at all temperatures, becoming increasingly negative to a relative value of about -1.3 % at T = 448 K.

Both of the literature data sets available for the CO_2-rich phase density of the $CO_2 + H_2O$ system were found to contain problems, either in the form of significantly larger data scatter [9] (±20 kg·m^{-3}) than the measurements in this work (±1.5 kg·m^{-3}), or in the form of systematic inconsistencies [10]. The new data reported here demonstrate that, for the conditions studied, the mass density of the saturated CO_2-rich phase is always within 8 kg·m^{-3} of the density of pure CO_2 at the same pressure and temperature. A maximum difference of about +8 kg·m^{-3} was observed to occur in the vicinity of the critical density of CO_2 at all temperatures, indicating that the increase in the molar density at these conditions arising from the presence of water made a larger contribution to the mass density than the associated decrease in the molar mass. Only at temperatures higher than about 423 K and at pressures below about 10 MPa was the mass density of the CO_2-rich mixture found to be unambiguously lower than that of pure CO_2 as might be expected from a consideration of ideal gas mixing. At densities above 800 kg·m^{-3}, the mixture density was less than 3 kg·m^{-3} above that of pure CO_2. For the CO_2-rich phase, the EOS-CG model [32] was able to describe the measured densities within ±5 kg·m^{-3}, with the deviations having a scatter comparable with the experimental uncertainty and exhibiting only slight systematic trends at higher temperatures. At temperatures of 373 K and above, the cubic EOS used in the model of Spycher and Pruess [18] was in suprisingly good agreement with the experimental data: its predictions of the maximum differences for the CO_2-rich phase densities from pure CO_2 ranged from (+6 to +11) kg·m^{-3} from (373 to 448) K, and it also correctly represented the observed behaviour in the limit of both high and low densities.

Acknowledgements

This work was carried out as part of the activities of the Qatar Carbonates & Carbon Storage Research Centre (QCCSRC). We gratefully acknowledge the funding of QCCSRC provided jointly by Qatar Petroleum, Shell, and the Qatar Science and Technology Park, and their permission to publish this research. The authors thank Roland Span, Monika Thol and Stefan Herrig at Ruhr-Universität Bochum for assisting with calculations made using the EOS-CG. EFM thanks the Department of Chemical Engineering and QCCSRC at Imperial College London for hosting him on his sabbatical where this work was done, and is grateful to everyone there who made that stay stimulating and enjoyable.

References

[1] K. Pruess, J. Garcia, Environmental Geology 42 (2002) 282-295.

[2] X. Li, E. Boek, G.C. Maitland, J.P.M. Trusler, Journal of Chemical & Engineering Data 57 (2012) 1078-1088.

[3] X. Li, E.S. Boek, G.C. Maitland, J.P.M. Trusler, Journal of Chemical & Engineering Data 57 (2012) 1369-1375.

[4] P.M. Haugan, H. Drange, Nature 357 (1992) 318-320.

[5] P.D. Jones, T.M.L. Wigley, P.B. Wright, Nature 322 (1986) 430-434.

[6] H. Teng, A. Yamasaki, M. Chun, H. Lee, Journal of Chemical Thermodynamics 29 (1997) 1301-1310.

[7] A. Hebach, A. Oberhof, N. Dahmen, Journal of Chemical & Engineering Data 49 (2004) 950-953.

[8] Z. Li, M. Dong, S. Li, L. Dai, Journal of Chemical & Engineering Data 49 (2004) 1026-1031.

[9] P. Chiquet, J. Daridon, D. Broseta, S. Thibeau, Energy Conversion and Management 48 (2007) 736-744.

[10] F.B. Tabasinejad, Yalda; Moore, Robert Gordon; Mehta, Sudarshan A.; Van Fraassen, Kees Cornelius; Rushing, Jay; Newsham, Kent Edward, Water/CO2 System At High Pressure And Temperature Conditions: Measurement And Modeling Of Density In Equilibrium Liquid And Vapor Phases., SPE EUROPEC/EAGE Annual Conference and Exhibition, SPE, Barcelona, Spain, 2010, pp. SPE-131636-MS.

[11] R. Yaginuma, Y. Sato, D. Kodama, H. Tanaka, M. Kato, Nihon Enerugi Gakkaishi 79 (2000) 144-146.

[12] J.A. Nighswander, N. Kalogerakis, A.K. Mehrotra, Journal of Chemical & Engineering Data 34 (1989) 355-360.

[13] Y.B. Chang, B.K. Coats, J.S. Nolen, SPE Reservoir Evaluation & Engineering (1998) 155-160.

[14] Z. Duan, R. Sun, C. Zhu, I. Chou, Marine Chemistry 98 (2006) 131-139.

[15] S.-X. Hou, G.C. Maitland, J.P.M. Trusler, Journal of Supercritical Fluids 73 (2013) 87-96.

[16] N. Spycher, K. Pruess, J. Ennis-King, Geochimica et Cosmochimica Acta 67 (2003) 3015-3031.

[17] N. Spycher, K. Pruess, Geochimica et Cosmochimica Acta 69 (2005) 3309-3320.

[18] N. Spycher, K. Pruess, Transport in Porous Media 82 (2010) 173-196.

[19] O. Redlich, J.N.S. Kwong, Chemical Reviews 44 (1949) 233-244.

[20] W. Wagner, A. Pruss, J Phys Chem Ref Data 31 (2002) 387-535.

[21] S. Al-Ghafri, G.C. Maitland, J.P.M. Trusler, Journal of Chemical & Engineering Data 58 (2013) 402-412.

[22] J. Sedlbauer, J.P. O'Connell, R.H. Wood, Chemical Geology 163 (2000) 43-63.

[23] Z. Duan, J. Hu, D. Li, S. Mao, Energy & Fuels 22 (2008) 1666-1674.

[24] D. Li, B.J. Graupner, S. Bauer, Energy Procedia 4 (2011) 3817-3824.

[25] M. McBride-Wright, G.C. Maitland, J.P.M. Trusler, Journal of Chemical & Engineering Data ASAP article (2015).

[26] M. McBride-Wright, Viscosity and Density of Aqueous Fluids with Dissolved CO_2, Chemical Engineering, Imperial College London, 2013.

[27] Z. Duan, N. Moller, J.H. Weare, Geochimica et Cosmochimica Acta 56 (1992) 2605-2617.

[28] Z. Duan, N. Moller, J.H. Weare, Geochimica et Cosmochimica Acta 56 (1992) 2617-2631.

[29] M. Benedict, G.B. Webb, L.C. Rubin, Journal of Chemical Physics 8 (1940) 334-345.

[30] R. Span, W. Wagner, J Phys Chem Ref Data 25 (1996) 1509-1596.

[31] O. Kunz, W. Wagner, Journal of Chemical & Engineering Data 57 (2012) 3032-3091.

[32] G.J. Gernert, R. Span, Journal of Chemical Thermodynamics (Submitted) (2015).

[33] H. Preston-Thomas, Metrologia 77 (1990) 3-10.

[34] E.F. May, W.J. Tay, M. Narnia, A. Aleji, S. Al-Ghafri, J.P.M. Trusler, Review of Scientific Instruments 85 (2014) 095111.

[35] D.O. Ortiz-Vega, K.R. Hall, J.C. Holste, V.D. Arp, E.W. Lemmon, Helmholtz equation of state for helium of Ortiz-Vega et al. (2013), 2013.
[36] W. Yan, S. Huang, E.H. Stenby, International Journal of Greenhouse Gas Control 5 (2011) 1460-1477.